Desalination and Water Treatment
www.deswater.com

doi:10.5004/dwt.2018.21742

103 (2018) 221–231
January

Hybrid nano-adsorbent supported carbon dots for removal of chromium from aqueous solution

Azadeh Eslami[a], Seyed Mehdi Borghei[b,*], Alimorad Rashidi[c], Afshin Takdastan[d]

[a]*Department of Environmental Engineering, Science and Research Branch, Islamic Azad University, Tehran, Iran, email: eslamiazade@yahoo.com (A. Eslami)*
[b]*Department of Chemical and Petroleum Engineering, Sharif University of Technology, Tehran, Iran, Tel. +982166005417, email: mborghei@sharif.edu (S.M. Borghei)*
[c]*Nanotechnology Research Center, Research Institute of Petroleum Industry (RIPI), Tehran, Iran, email: rashidiam@ripi.ir (A. Rashidi)*
[d]*Department of Environmental Health and Environmental Technologies Research Center, Ahvaz Jundishapur University of Medical Sciences, Ahvaz, Iran, email: afshin_ir@yahoo.com (A. Takdastan)*

Received 26 July 2017; Accepted 24 November 2017

ABSTRACT

In this study, hybrid nano adsorbent supported carbon dots was prepared and used for removing Cr(VI) from aqueous solution. Carbon dots were synthesized from sugarcane molasses under microwave irradiation. Hybrid nano adsorbent was prepared by impregnating carbon dot with H_3PO_4 in a ratio of 2:1 and introducing 0.01 M $FeCl_3$ into the slurry. The carbon dot hybrid was activated via a conventional thermal method under N_2 flow. The physico-chemical properties of the synthesized material were investigated using X–ray diffraction (XRD), Fourier transform infrared spectroscopy (FTIR), N_2 adsorption/desorption, and field emission scanning electron microscopy (FESEM). Chromium adsorption was studied in a synthesized aqueous solution using hybrid Fe–carbon dots as the adsorbent under various adsorption conditions like solution pH, adsorbent dosage, various initial chromium concentrations, and contact time. Adsorption isotherms were conducted and it was indicated that the adsorption equilibrium data was well fitted for both the Langmuir ($R^2 > 0.99$) and Freundlich ($R^2 > 0.97$) models. The maximum adsorption capacity of Cr(VI) onto Fe–CDs was obtained at 81.97 mg g^{-1}. Adsorption kinetics for Cr(VI) was followed. The pseudo-second-order model indicated very well that the rate-controlling step in the adsorption is mainly chemisorption. The saturated hybrid nano adsorbent could be easily regenerated using dilute 1 N NaOH and 1 N HCl aqueous solutions and high desorption efficiency (up to 74%) of Cr(VI) was achieved for various initial chromium concentrations after 5 adsorption-desorption cycles. The obtained results proved that the hybrid Fe–CDs is a low–cost and effective adsorbent for Cr(VI) ions removal.

Keywords: Carbon dots; Hybrid Fe–carbon dots; Nano adsorbent; Hexavalent chromium; Aqueous solution

1. Introduction

Nowadays, heavy metal pollution is one of the greatest environmental and health problems across the world [1–4]. Chromium is a primary metal pollutant, which is discharged into the aquatic environment by modern civilization. Chromium is released into the environment through metal processing, mining, leather tanning, electroplating, pigment synthesis, wood protection, electrical and electronic equipment, plastic and cement industries, dyeing, fertilizer, etc. [5–7]. Chromium mainly exists in both trivalent and hexavalent forms, of which hexavalent chromium is highly toxic and can cause severe damage to public health such as dermatitis, kidney circulation disorders, lung cancer, and, finally, death, even at low concentrations [6,8,9]. Due to the non-biodegradability, toxicity, and mobility of Cr(VI) in water bodies and bio accumulation in living cells [10,11], the maximum accept-

*Corresponding author.

able concentration of Cr(VI) is limited to 50 μg L^{-1} by the US EPA [12,13]. During the past decades, a variety of methods including chemical precipitation, membrane separation, ion exchange, electrochemical approaches, electro dialysis, photo catalytic degradation, reverse osmosis, ultra filtration, and adsorption have been utilized for the treatment of Cr(VI) in contaminated water [6,14–18]. However, most of these methods have some drawback; they are often used in many water and wastewater treatment utilities for chromium removal. Chemical precipitation produces a large amount of precipitate sludge during the process as well as involves extra processes for further treatment. A number of disadvantages limits the application of membrane separation such as high operational cost and limited pH range. Operational cost is often a limiting factor for the application of ion exchange in metal ions removal. Totally, the deficiencies of low feasibility of scale-up for industrial purposes, ineffectiveness at high concentrations, secondary pollution, cumbersome procedures, and high operational cost exist in most of the above-mentioned chromium removal methods [9,11,18,19]. Among diverse methods for removing toxic heavy metals, adsorption is generally recognized as the most effective and reliable approaches due to its high flexibility, cost-effectiveness, easy handling, high efficiency, simplicity of design, low energy consumption, and environmental friendliness in comparison with other conventional methods [6,20,21].

Compared with traditional adsorbents such as activated carbon [4], activated alumina, biosorbents, synthetic polymers, and silica-based materials [22], nanosorbents are desirable because of their small particle size, high specific surface area, large pore volume, and controllable morphology that improve chemical reactivity and adsorbate/adsorbent interactions [23–25] and enhance the removal of contaminants over a broad concentration range (~1–1000 ppm) in a short time [26].There are ongoing efforts to fabricate nano particles that improve its physical properties and chemical functionalities, and promote its performance in application [27]. There is also a need to investigate for new nano particles that are nontoxic, more sustainable, environment-friendly and synthesized easily according to green production procedures using renewable precursors [27–29]. Considering the above properties, high surface area, and effective functional groups for removing a variety of organic and inorganic contaminants, carbon nano dots should be promising to turn into alternative materials for water remediation. However, due to high solubility of carbon dots, there are few reports for the use of these materials as an adsorbent [30]. To overcome this property, some researchers employed different strategies like: gold nano particles as supports [31]; functional groups such as magnetic ferrite–MOS_2 [32]; modification with Mesoporous organo silica [33]; decorating supported carbon dots with metallothionein [22] and Silica nano particles [34]; composition of carbon dots with layered double oxide/hydroxide materials [30,35], TiO_2 nano particles [36], chitosan hydrogel [37], mesoporous silica nano particles [38] and multiwalled carbon nanotubes [39]. However, though the procedures mentioned above are successful in the adsorption process, it is still necessary to exploit a novel carbon dot-based adsorbent material for the betterment of adsorption behavior and efficiency of carbon dots especially, using cost effective precursors. Activation using physical and chemical ways is common for the production of activated carbon and, recently, some efforts have been conducted to activate carbon nanotubes [40–42]. The activation process is carried out during physical and chemical procedures. Physical activation include carbonization of carbonaceous materials at high temperature (500–900°C) followed by thermal activation in an inert atmosphere or pyrolysis at elevated temperatures in the presence of air, steam, and carbon dioxide [43]. In contrast, chemical activation is carried out in the presence of activation agents such as phosphoric acid, $ZnCl_2$, KCl, $AlCl_3$, $MnCl_2$, $CuCl_2$, and $FeCl_3$, while pyrolysis and activation are performed in only one stage [44–47]. Often, chemical activation is preferred as it produces larger pore structure than physical activation methods, enabling the adsorption of higher molecular size adsorbates [48,49]. Utilization of phosphoric acid as the activation agent for synthesis of activated carbon from agricultural waste has been widely established in the literature [46,50–52]. Although, due to the surprising properties of carbon dots, synthesis and application of CDs nano composites is ongoing, however, to the best of our knowledge, no study has been focused on the activation of carbon nano-dots prepared from green precursor, and using activation agents in order to formation of pore, improvement of the adsorption capacity and reduction of water solubility. In this research work, the rapid synthesis of carbon nano dots from sugarcane molasses with microwave irradiation is carried out. Synthesis of hybrid nano adsorbent is reported for the first time by employing H_3PO_4 and $FeCl_3$ as activation agent, thermal carbonization as the heating method, and evaluated the ability of hybrid Fe–CDs to adsorb Cr(VI) from aqueous solutions. To study the influences of the assisted activator on carbon dots, hybrid Fe–CDs were characterized by N_2 adsorption, X–ray diffraction (XRD), Fourier transform infrared spectroscopy (FTIR), and field emission scanning electron microscopy (FESEM). The adsorption isotherm and kinetics of Cr(VI) from aqueous environment on Fe–CDs are also studied to comprehend the adsorption mechanism. The saturated hybrid Fe–CDs is regenerated and reused for removing various Cr(VI) concentrations.

2. Materials and methods

2.1. Materials

All the chemicals and reagents were of analytical grade. Ferric chloride ($FeCl_3{\cdot}6H_2O$) of purity 99.9%, phosphoric acid (85%), NaOH, HCl, and $K_2Cr_2O_7$ were purchased from Merck. Sugarcane molasses was prepared from Karun Agroindustry of Khuzestan. Stock solution of Cr(VI) (100 mg L^{-1}), was prepared by dissolving 0.1414 g of $K_2Cr_2O_7$ in 500 ml double distilled water. Ultrapure water was prepare dusing Milli-Q water purification system. Atomic absorption spectrometer (model AAnalyst 700, Perkin Elmer) at 357.8 nm wavelength, was used for determining the hexavalent chromium concentration.

2.2. Preparation of carbon dots

Carbon dots were synthesized using a domestic microwave oven (900W, 100% of total power) according to the Das et al. method with some modification [26]. Typically, 30 grams of sugarcane molasses was dissolved in 100 ml of Mil-

li-Q water and stirred for 1 h. The pH of the solution was adjusted to the alkaline condition (pH = 11) using NaOH 1 M. The solution was irradiated for 3.5 min and centrifuged for 10 min in 12,000 rpm to remove the large aggregates. The pH of the clarified solution was reduced to seven by the addition of 0.1 M HCl and dried overnight in vacuum oven at 110°C. Optimization of the parameters for synthesis of CDs was obtained by performing the synthesis with varying pH values, irradiation time, and precursor concentration.

2.3. Preparation of hybrid Fe–CDs

Specially, 10 g of synthesized carbon dots was mixed with 0.01 M $FeCl_3{\cdot}6H_2O$ and H_3PO_4 in the ratio of 2:1 (activator to precursor ratio) to form slurries. For as much as H_3PO_4 concentration is a key factor in the activation process, many researchers reported greater surface area and porous structure at the optimum impregnation ratio (weight of biomass: weight of H_3PO_4) of 1:1, 1:1.5, 1:2, and 1:3 [48,49,53]. The mixture was kept at room temperature and stirred for 12 h. The wet samples were transferred into an oven and dried overnight at 110°C. For the carbonization of impregnated samples, the resulting dried composite materials were put in aceramic boat and transferred into a tubular furnace. Pyrolysis was conducted at 550°C for 1 h with a heating rate of 10°C min^{-1} under a high purity nitrogen flow of 100 ml min^{-1}. After cooling to room temperature, the obtained material was washed repeatedly with hot deionized water until it reached a constant pH, filtered, and dried at 110°C for 24 h. The dried substances were cooled and stored in a dark place for the next analysis.

2.4. Characterization

The surface morphologies of carbon dots and hybrid Fe–carbon dots were determined by FESEM(TESCAN MIRA3, LMU) after coating the particles with gold film. SEM/EDX analysis was conducted to determine the elemental compositions of nano adsorbent before and after the adsorption experiments.

The FTIR-used pellets in the range of 600–4000 cm^{-1} for virgin and spent Fe–carbon dot, were recorded on a Bruker Tensor 27 spectrometer. Chemical composition and molecular structure of synthesized hybrid nano adsorbent before and after the adsorption of Cr(VI), were analyzed using this method.

The textural properties of the Fe–carbon dot including pore structure and surface area, were determined using an accelerated surface area and porosimetry system (ASAP 2020 micro meritics), and N_2 adsorption at 77 K. The BET (Brunauer-Emmett-Teller) equation was used for the calculation of specific surface area (S_{BET}), total pore volume (V_T) and average pore diameter (D_p). The micropore surface area (S_{mic}) and micropore volume (V_{mic}) were evaluated using the t-plot method. The external volume (V_{ext}) obtained from the deduction of V_{mic} from V_T and the external area (S_{ext}), was acquired from the deduction of S_{mic} from S_{BET}. According to the following equation, the average pore size (r) was estimated:

$$r = \frac{4V_t}{S_{BET}} \tag{1}$$

X–ray diffraction (XRD) (model PW3830, Philips) patterns with Ni-filtered Cu-Kα radiation as the X–ray source were scanned for 2θ = 5°–80°.

2.5. Adsorption and desorption experiments

The adsorption experiments of Cr(VI) were conducted by batch mode in 80 mL Nalgene polypropylene bottles at room temperature. For each time, 0.045 g Fe–carbon dot was added to a 30 ml solution containing 10, 30, 50, 75, and 100 mg L^{-1} Cr(VI), prepared using $K_2Cr_2O_7$ as the source, at initial pH of 2, and shaken in a thermostat shaker at 180 rpm for different times (1, 10,20,30,60,90,120, 180, 240, and 300 min). The effect of initial pH on the adsorption of Cr(VI) was carried out by adding 0.045 g of adsorbent to the series of bottles containing 100 mg L^{-1} Cr(VI) at pHs ranged from 1 to 9. The pH adjustment was done using dilute sodium hydroxide and sulfuric acid standard solutions. Hexavalent chromium determination was performed using Atomic Adsorption Spectroscopy. The effect of hybrid Fe-CDs dosage on the adsorption of hexavalent chromium was investigated by adding 0.015, 0.03, 0.045, 0.06, 0.075, 0.09, and 0.15 g of adsorbent and stirring the bottles containing 100 mg L^{-1} Cr(VI) with the initial pH of 2 for 180 min at room temperature.

The equilibrium adsorption capacity, q_e (mg g^{-1}), was calculated by measuring Cr(VI) concentration before and after the adsorption using Eq. (2):

$$q_e = \frac{(C_0 - C_e)V}{m} \tag{2}$$

where C_0 and C_e (mg L^{-1}) are the initial and equilibrium concentration of Cr(VI) in aqueous environment respectively, V (ml) is the volume of chromium solution, and m (mg) is the mass of the hybrid Fe–CDs.

In the desorption experiments, the loaded Fe–CDs adsorbent with Cr(VI) ions were first treated with 50 ml of 1 N NaOH solution for 360 min, then filtered and washed with DD water. Further regeneration was carried out using 50 ml of 1 N HCl for regeneration of sorption sites [54]. After that, hybrid Fe–CDs was washed with DD water several times and dried overnight. The quantity of Cr(VI) released from hybrid Fe–CDs into the aqueous solution was examined using Atomic Adsorption Spectroscopy. Desorption studies was conducted for five consecutive adsorption-desorption cycles at various concentrations of Cr(VI) ranges from 10 to 100 mg L^{-1} at optimum experimental condition.

3. Results and discussion

3.1. Characterization

The FTIR spectra of the hybrid Fe–carbon dot before and after Cr(VI) adsorption, is demonstrated in Fig. 1. The wave number at 2928 cm^{-1} and 2857 cm^{-1} corresponds to the bonds of C–H stretching vibration in alkanes. The spectrum at 1580 cm^{-1} is assigned to C=O stretching vibration of carboxylic acids. These absorption bond peaks shift towards lower than 1600 cm^{-1} wave numbers, if the C=C bond is conjugated in an aromatic ring, or a C=O bond [53]. The bond about 1117 cm^{-1} and 1160 cm^{-1} belongs to stretching vibration of C–O in

phosphate esters. Generally, the absorption of energy in the peaks at 1000–1300 cm^{-1}, can be attributed to the C–C and C–O vibration in acids, alcohols, phenols, ethers and esters [45,53,55]. Also, it is a clear evidence for the existence of phosphorous and phosphor containing carbonaceous materials in the carbon dots activated with the phosphoric acid [56]. The strong absorption bands at 970 cm^{-1} and 877 cm^{-1} corresponds to =C–H out-of-plane in the spectra of alkenes and C–H out-of-plane which are characteristic of the aromatic substitution pattern, respectively. Totally the strongest bands in the spectra of alkenes are those ascribed to the carbon–hydrogen bending vibrations of the =C–H group. These bands are in the region 650–1000 cm^{-1}. Low transmittance intensity and the shifted peak locations at different wave numbers for the FTIR spectra of Cr(VI) loaded nano adsorbent is due to chromium adsorption. It clearly indicated that functional groups corresponds to adsorption process.

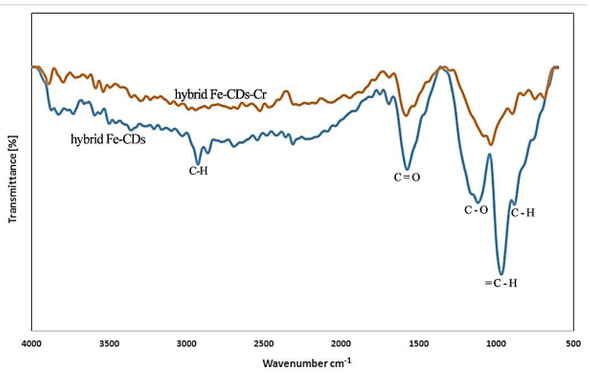

Fig. 1. FTIR spectra of hybrid Fe–carbon dots before and after of the Cr (VI) adsorption.

The surface morphology of the synthesized hybrid Fe–carbon dots was confirmed using field emission scanning electron microscopy. Fig. 2 demonstrates the FESEM images of carbon dots and hybrid nano adsorbent. FESEM image of carbon dots (Fig. 2a) clearly depicted that it is possible to synthesize nono-sized carbonaceous materials from sugarcane molasses. As indicated in Fig. 2b, the surface morphology of the hybrid Fe–carbon dots is partially rugged with mesoporous structure. Obviously, it can be observed that the size distribution of the nano particles are uniform and in the range of 10–20 nm. Elemental composition of the carbon dot and hybrid nano adsorbent was determined using EDX spectrum. Fig. 3 and Table 1 demonstrate this EDX analysis.

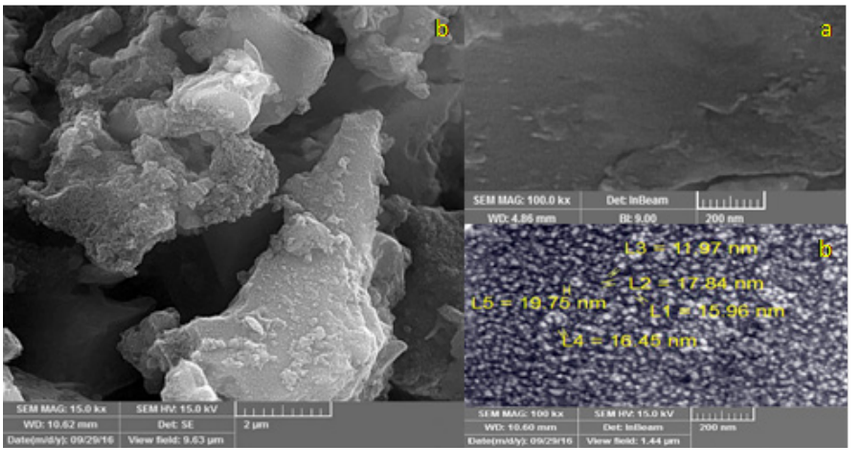

Fig. 2. FESEM images of (a) carbon dots, (b) hybrid Fe–carbon dots.

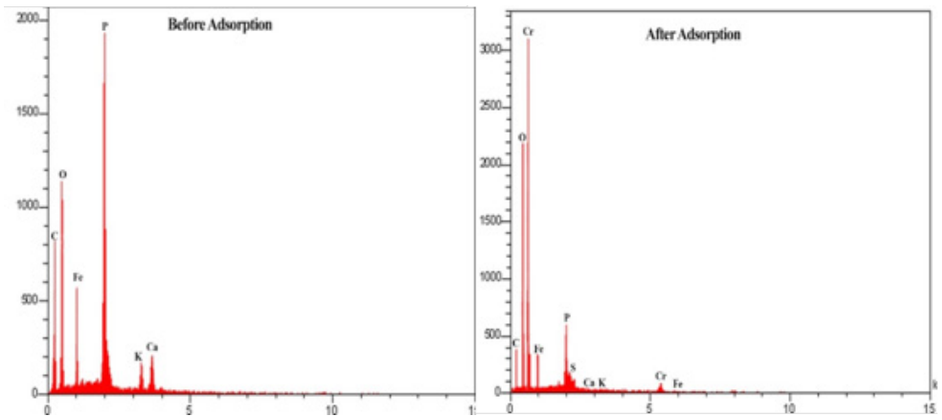

Fig. 3. EDX spectra of hybrid Fe–carbon dots before and after of the Cr (VI) adsorption.

Table 1
Elemental composition of carbon dot, hybrid Fe–CDs before and after adsorption

Elements	Carbon dot		Hybrid Fe-Carbon dots		Hybrid Fe-Carbon dots + C(VI)	
	(Wt–%)	(A–%)	Wt (%)	A (%)	Wt (%)	A (%)
C	36.03	39.71	61.30	69.97	61.38	70.47
O	60.21	58.51	25.13	22.23	20.87	17.78
P	–	–	10.20	6.76	10.03	5.93
Na	3.23	1.58	0.59	0.20	0.5	0.17
S	0.43	0.17	0.39	0.14	0.19	0.11
Fe	–	–	0.89	0.45	0.69	0.32
Au	0.1	0.03	1.5	0.25	1.5	0.25
Cr	–	–	–	–	4.84	3.97

Carbon dots contain considerably high oxygen content partially due to the presence of carbonyl groups [27]. The most elements for hybrid Fe–CDs exhibit carbon (61.3%) and oxygen (25.13%) depending on the carbon dots basis of the adsorbent. Phosphorous (10.2%) was also found because of phosphoric acid used for activation. Small amounts of iron corresponding to ferric chloride were added during synthesis of hybrid Fe–CDs. The peak of chromium indicated that this element was successfully adsorbed.

The textural properties of hybrid Fe–CDs such as surface area and pore volume, Brunauer-Emmett-Teller (BET) surface area, and pore volume measurements were evaluated particularly. Figs. 4a, b depict the N_2 adsorption-desorption isotherms and pore size distribution curves of hybrid Fe–CDs respectively. As indicated in Fig. 4a, the adsorption–desorption isotherm is classified as type IV with H_3 hysteresis loop in the P/P_0 range of 0.45–1.0, characteristic of mesoporous material with slip-shaped pores, which at high P/P_0, do not appear to be any limiting adsorption [30,57]. The specific surface area of carbon dot and hybrid Fe–CDs is calculated to be 2.14 $m^2 g^{-1}$ and 233.7 $m^2 g^{-1}$ respectively, using BET. The average pore size of 33.5 nm is obtained from the desorption section using Barrett-Joyner-Halenda (BJH) model, in which the pore size distribution is centralized in the mesopore range. BJH pore size distribution of hybrid Fe–carbon dots is shown in Fig. 4b. The obtained data confirmed that, this hybrid material is mesopore dominated with scarce micropore portion to its total surface area. Other structural properties of hybrid Fe–CDs are summarized in Table 2.

The X-ray diffraction pattern of carbon dots and hybrid Fe-carbon dots before and after adsorption is shown in Fig. 5. The XRD pattern of carbon dot shows some graphite-like peaks at 30, 35, 40°. A broad peak around 20–40° which is due to the oxygen containing groups located at the surface of the layer of the carbogenic core, indicating poor crystalline nature of CDs. The XRD pattern of hybrid Fe–CDs before adsorption indicated a broad peak near 24° with a high intensity. This reveals the amorphous patterns of the synthesized adsorbent. Furthermore, no significant peak for iron was observed because of low Fe concentration in hybrid nano adsorbent. As indicated, the XRD pattern after the adsorption of Cr(VI) did not show any significant changes, which represented that the structure of the adsorbent was protected during the adsorption process.

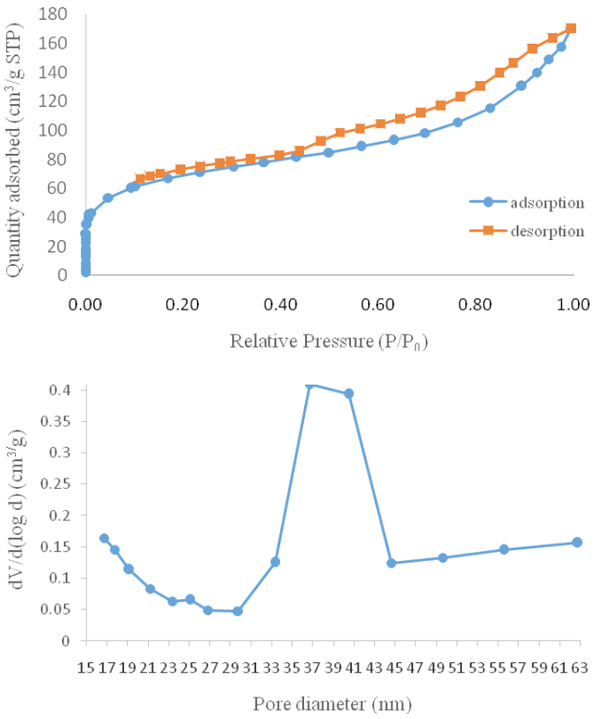

Fig. 4a. N_2 adsorption/desorption isotherms of hybrid Fe–carbon dots, b. BJH pore size distribution curve of hybrid Fe–carbon dots.

Table 2
Structural parameters of hybrid Fe–carbon dots

Sample	Fe-CDs
S_{BET} ($m^2 g^{-1}$)[a]	233.7
S_{ext} ($m^2 g^{-1}$)[b]	196.2
V_{total} ($cm^3 g^{-1}$)[c]	0.26
V_{mic} ($cm^3 g^{-1}$)[d]	0.02
D_{BJH} (nm)[e]	33.5

[a]BET surface area, [b]t-plot external surface area, [c]Total pore volume of pores, [d]t–plot Micropore volume, [e]BJH desorption average pore diameter.

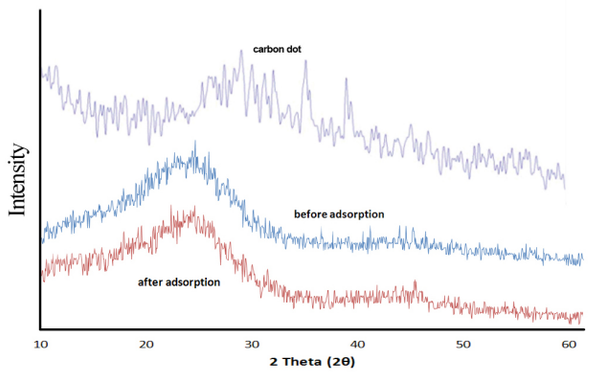

Fig. 5. XRD patterns of carbon dots and hybrid Fe–carbon dots before and after of the Cr(VI) adsorption.

3.2. Influence of pH

The pH of a solution is a significant controlling parameter in the metal ions adsorption process. It has a strong effect on the active surface binding sites and functional groups of adsorbent as well as aqueous chemistry of the solution. The influence of the initial pH of the solution on the adsorption of Cr(VI) onto hybrid Fe–CDs was shown in Fig. 6. The pH of Cr(VI) solution varied from 1.0 to 9.0 at initial chromium concentration of 100 mg L^{-1}. As indicated in Fig. 6, the adsorption capacity decreased with increasing pH, with the maximum adsorption at pH = 2.0. The reason for this pH-depended adsorption capacity may be attributed to the dependency of the Fe–CDs adsorbent for the various species of Cr(VI) in the forms of $H_2CrO_4^0$, $HCrO_4^-$, CrO_4^{2-} and $Cr_2O_7^{2-}$ in acidic conditions [6]. Under acidic pH, the carbon surface of the Fe–CDs can be protonated by the community of H^+ ions, which is favorable for electron attraction of negatively charged $HCrO_4^-$, $Cr_2O_7^{2-}$ to positively charged carbon nano dots in the adsorption process. At pH = 1, hexavalent chromium mostly exist as H_2CrO_4 and $HCrO^-$ while at pH of 2.0, $HCrO^-$ species are abundant; so, higher adsorption is expected. As pH increased from 2.0 to 9.0, the $HCrO_4^-$ converts to CrO_4^{2-} gradually. The electron repulsion between such negative species of Cr(VI) and negatively charged carbon nanoparticles increased under weak acidic conditions, which result in the reduction of Cr(VI) adsorption [58]. As the highest adsorption capacity occurs at pH of 2.0, all the experiments are conducted at this pH value.

3.3. Adsorption isotherms

The maximum loading capacity of the adsorbent versus equilibrium adsorption concentration can be described with the adsorption isotherms. The effect of initial adsorbate concentration (ranging from 10 mg/L to 100 mg/L) on chromium adsorption capacity is represented in Fig. 7. The adsorption capacity of the hexavalent chromium onto activated carbon dots increased with increasing of initial Cr(VI) concentration, which may be because of the abundance of Cr(VI) ions in the solution, greater driving force to dominate mass transfer resistances, and increasing the chance of clashes with the active sites [59]. For better realization of the correlation between the adsorbate concentration and adsorbent, the two most frequently used adsorption isotherm models are Langmuir [60] and Freundlich [61], developed to interpret incoming experimental data of Cr(VI) adsorption on to hybrid Fe–carbon dots. Langmuir isotherms, which are applicable to the homogeneous adsorption surface with equal adsorbate affinity sites [34] and assumes mono layer adsorption [62,63], is explained with the following linear equation [22,64]:

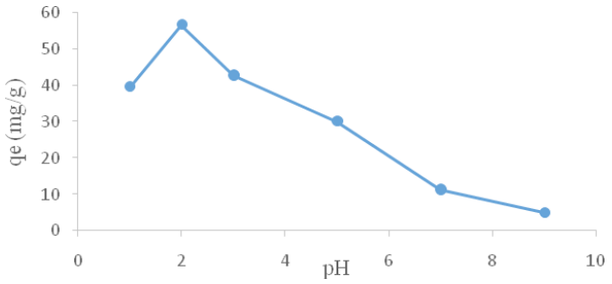

Fig. 6. Effect of pH on the adsorption of Cr(VI) onto Fe–CDs, (Fe–CDs = 1.5 g L^{-1}, initial Cr(VI) concentration = 100 mg L^{-1}).

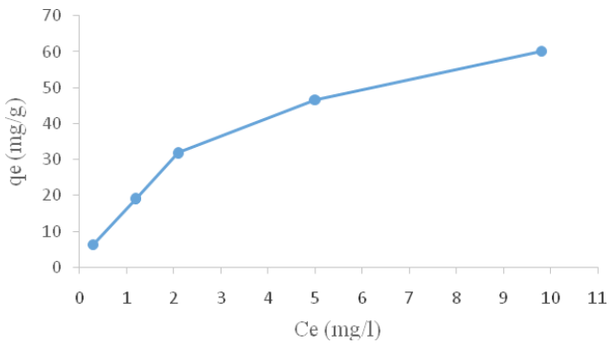

Fig. 7. The influence of adsorbate concentration on Cr(VI) adsorption capacity (pH = 2, V = 30 ml, Fe-CDs = 1.5 g L^{-1}).

$$\frac{C_e}{q_e} = \frac{1}{bq_m} + \frac{C_e}{q_m} \tag{3}$$

where C_e (mg/L) is the equilibrium adsorbate concentration in solution, q_e (mg/g) is the amount of metal ions adsorbed on Fe–CDs at equilibrium, q_m (mg/g) is the maximum capacity of the mono layer adsorption, and b (L/mg) is the Langmuir constant. In addition, b illustrates the association between solute and adsorbent binding sites [62]. Another key dimensionless parameter R_L, that is expressed by the following equation, can be calculated from Langmuir model [58].

$$R_L = \frac{1}{1 + bC_0} \tag{4}$$

where R_L is the dimensionless Langmuir constant, and C_0 (mg/L) is the initial Cr(VI) concentration. The value of R_L represents the type of isotherm which is irreversible ($R_L = 0$), favorable ($0 < R_L < 1$), linear ($R_L = 1$) and unfavorable ($R_L > 1$) [34]. According to the experimental data in this study, the R_L parameter at initial Cr(VI) concentrations of 10, 30, 50, 75, and 100 mg/L was calculated to 0.26, 0.11, 0.07, 0.045 and

0.034 respectively. Comparing the results to the separation factor (R_L) indicated that the Langmuir isotherm was found to be favorable. The values of q_{max} and b in the Langmuir isotherm plot (Fig. 8) can be specified from the slopes and intercepts of the plot of C_e versus C_e/q_e respectively.

Another important method for describing the adsorption onto heterogeneous surface based on multilayer sorption assumption and uniform distribution of energy, is the Freundlich model;the linear type of this isotherm for reversible adsorption is as follows [64]:

$$\log q_e = \log K_f + \frac{1}{n}\log C_e \quad (5)$$

where K_f [(mg/g) (L/mg)$^{1/n}$] and n are the Freundlich constants and indicate adsorption capacity and adsorption intensity, respectively.

According to Fig. 9, the values of 1/n and K_f in the Freundlich isotherm plot were specified from the slope and intercept of the plot of log C_e against log q_e, respectively.

The obtained values from the Langmuir and Freundlich isotherms that were assessed by the linear approach of the experimental data are summarized in Table 3. As indicated, the experimental data were fitted very well with both Langmuir and Freundlich isotherms based on R^2 values, which is ascribed to the homogeneous surface of the hybrid Fe–carbon dots and mono layer adsorption. As well as the Freundlich constant, the value of 1/n being less than 1, corroborates the favorable adsorption of Cr(VI) on the synthesized adsorbent.

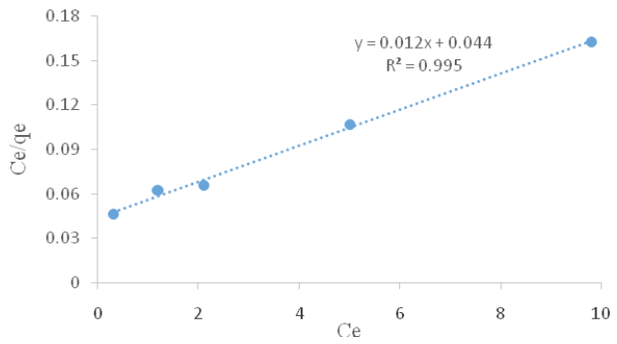

Fig. 8. Langmuir isotherm of Cr(VI) adsorption on hybrid Fe–carbon dots.

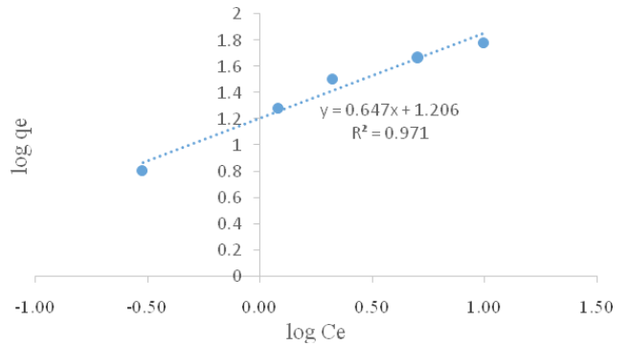

Fig. 9. Freundlich isotherm of Cr(VI) adsorption on hybrid Fe–carbon dots.

3.4. The effect of reaction time and adsorption kinetics

The equilibrium adsorption of Cr(VI) on hybrid Fe–CDs versus time profile for various Cr(VI) concentrations is presented in Fig. 10. From the economical and practical viability standpoint, equilibrium reaction time and adsorption capacity of the adsorbent are the two key factors for adsorption surveys. From Fig. 10 it can be perceived that the adsorption capacity of the adsorbent increases with increasing initial Cr(VI) concentration. This is due to the fact that at higher initial chromium concentrations, more number of metal ions is available for adsorption, and it develops higher diving force to dominate the resistance against mass transfer of the metal ions between the aqueous and solid phase [2,34]. In addition, it is realized that the equilibrium adsorption of Cr(VI) onto hybrid Fe–CDs occurred initially fast and then gradually slowed according to obtained experimental data. During the rapid step (the first 30 min) for initial concentration ranges from 10 to 100 mg/L, about 70% of Cr(VI) adsorption is happened, which may be because of the fast diffusion of metal ions from aqueous solution to the external surface of the adsorbent [65]. Since the outer surface area per unit mass increased in nano scale adsorbents, most of the active sites are presented on the exterior surface of the nano adsorbent and are easily available for adsorbate molecules [34,66]. Gradual adsorption in the latter time duration is probably due to the diffusion of the Cr(VI) ions into the porous structure of the hybrid Fe–CDs [65]. The adsorption equilibrium happened in 90 min for all initial Cr(VI) concentrations in this study.

For understanding the kinetics adsorption mechanism of Cr(VI) on hybrid Fe–CDs, both pseudo-first-order and pseudo-second-order kinetic models were used to fit the

Table 3
Langmuir and Freundlich parameters for the adsorption of Cr(VI) onto hybrid Fe–carbon dots

Isotherm	Parameters	Value
Langmuir	q_m, (mg/g)	81.97
	b	0.277
	R^2	0.996
Freundlich	$1/n$	0.647
	K_f (mg/g)(L/mg)$^{1/n}$	16.077
	R^2	0.971

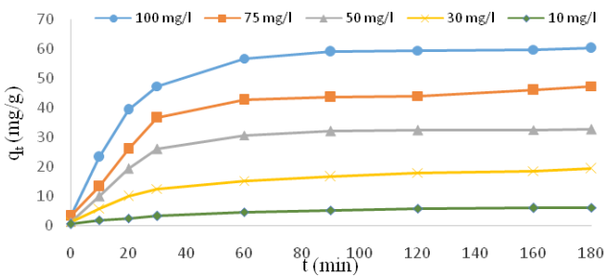

Fig. 10. Time profile of Cr(VI) adsorption on hybrid Fe–carbon dots for different initial chromium concentration.

esulting data. These kinetic models can be characterized using Eqs. (6) and (7), respectively [2,58,66].

$$\log\left(q_e - q_t\right) = \log q_e - \frac{k_1}{2.303}t \tag{6}$$

$$\frac{t}{q_t} = \left[\frac{1}{k_2 q_e^2}\right] + \frac{t}{q_e} \tag{7}$$

where q_e (mg/g) represents equilibrium adsorption capacity, q_t (mg/g) is the amount of Cr(VI) adsorbed at time t, k_1 (1/min) and k_2 (g/(mg min)) are the pseudo-first-order and pseudo-second-order rate constant, respectively.

Figs. 11 and 12 depict the pseudo-first-order and pseudo-second-order model plots that the kinetic parameters ere specified from the intercept and slope of linear line for the plot of log (q_e–q_t) and t/q_t against t, respectively. Using Eq. (8), the initial adsorption rate (V_0) can be calculated from rate constants of the t/q_t vs. t plot of pseudo-second-order model [34,67].

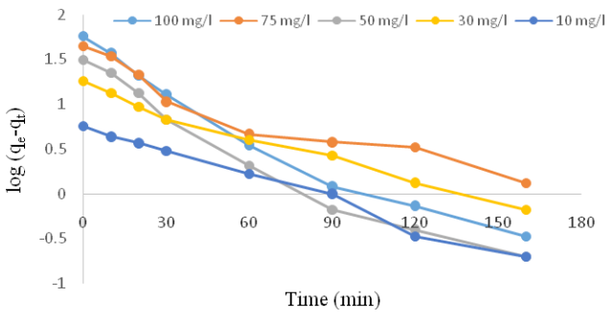

Fig. 11. Pseudo–first–order kinetics of Cr(VI) on hybrid Fe–carbon dots.

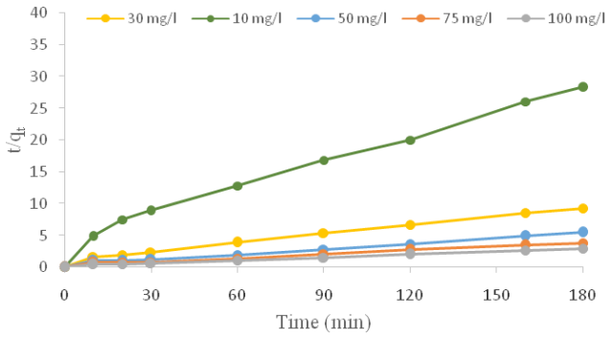

Fig. 12. Pseudo–second–order kinetics of Cr(VI) on hybrid Fe–carbon dots.

$$V_0 = k_2 q_e^2 \tag{8}$$

Mostly, pseudo-first-order kinetics does not conform for the whole ranges of reaction time and probably is more appropriate for the initial stage of the adsorption processes. Besides, the calculated Q_e values from this model are in a relatively poor conformation with the obtained data from the experiment ($Q_{e,exp}$) at different chromium concentrations. Table 4 shows the correlation coefficients and different kinetic parameters of both the models.

According to the table, correlation coefficient (R^2) obtained from the pseudo-second order model are high as compared to the pseudo-first order model. Also, for the pseudo-second order model, the calculated Q_e values agree with the experimental data. Totally, pursuant to all these, the adsorption of Cr(VI) onto hybrid Fe–CDs behaves according to the pseudo-second order models. Prosperous agreement of the obtained data with the pseudo-second-order kinetic indicates that the rate-controlling step in the adsorption is mainly chemisorption [2,34,65,68], which occurred probably owing to exchange of electrons between hybrid Fe–CDs and Cr(VI) ions [6]. Table 5 indicates the comparison of BET surface area, pH, Q_{max} and equilibrium time for Cr(VI) adsorption on different adsorbents. Comparing the obtained data from different literature establishes the fact that hybrid Fe–CDs with a not very high surface area, also has a good adsorption capacity and fast adsorption rate as compared to other adsorbent materials. It suggests that this kind of process cannot be described just by considering the surface area. Li et al. and Dutta et al. reported that graphene oxide shows higher adsorption capacity as compared to carbon nanotube; however, it has lower surface area than CNT. Although, the surface area is a key factor in the adsorption process, it seems that the diffusion resistance also is a determinant agent in adsorption rate and capacity [34] .

3.5. Desorption experiments

The loaded nano adsorbent, which contains various amounts of Cr(VI), cannot be disposed to the environment

Table 4
Kinetic constants for the adsorption of Cr(VI) onto hybrid Fe–carbon dots

C_0 (mg/l)	Pseudo-first-order model parameters				Pseudo-second-order model parameters			
	$q_{e,cal}$ (mg/g)	$q_{e,exp}$ (mg/g)	K_1 (1/min)	R^2	q_e (mg/g)	K_2 (g/(mg min))	R^2	V_0 (mg/g min)
10	5.67	6.33	0.021	0.989	7.0	0.0061	0.977	0.3
30	14.84	19.33	0.0198	0.987	20.66	0.0028	0.988	1.19
50	22.9	32.73	0.033	0.959	35.09	0.0024	0.990	2.95
75	30.08	47.33	0.02	0.910	50.25	0.0014	0.988	3.6
100	39.3	60.13	0.033	0.963	63.29	0.0017	0.995	7.05

Table 5
Comparative investigation of Cr(VI) adsorption capacity using hybrid Fe–carbon dots with previously reported adsorbents

Adsorbent	S_{BET} ($m^2 g^{-1}$)	Adsorbent concentration (g L^{-1})	pH	Equilibrium time (min)	Q_{max} (mg g^{-1})	Reference
THAC-Fe	920.13	1.5	2–3	90	11.83	[9]
Magnetite Nanoparticles	12.7	2	2	1500	20.2	[5]
AC-Fe	1156	1	5.38	800	34.39	[45]
Fe/CCMs-800	N.R*	1	3	120	75.3	[21]
N-enriched AC	1511	0.1	2	540	137	[69]
Mesoporous carbon microspheres	1061	0.2	3	1440	139	[6]
Mango kernel activated carbon	490.43	2.5	2	150	7.8	[70]
Hybrid Fe-CDs	234	1.5	2	90	81.97	This study

*Not reported

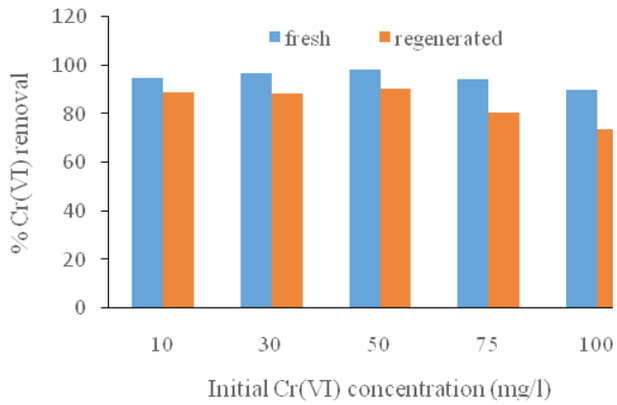

Fig. 11. Pseudo–first–order kinetics of Cr(VI) on hybrid Fe–carbon dots.

because of environmental protection requirements and restrictions. In addition, regeneration and reuse of the adsorbent develops its cost-effectiveness for the removal of Cr(VI) ions. As mentioned, Cr(VI) adsorption was conducted at different initial concentrations of 10 to 100 mg L^{-1}. Then, desorption studies were carried out at the same Cr(VI) concentrations. Fig.13 shows the percentage of Cr(VI) removal using fresh and regenerated hybrid Fe–CDs adsorbent at various concentrations of Cr(VI). The figure clearly indicated that Cr(VI) removal varies from 98.2% to 90.21% for fresh hybrid Fe–CDs as compared to values corresponding to regenerated adsorbent ranging from 90.45% to 74% after 5 consecutive adsorption-desorption cycles. The obtained results in this study show that it is possible to regenerate and reuse the hybrid Fe–CDs. It is concluded that the adsorption of Cr(VI) onto hybrid Fe–CDs is an example of physical adsorption and depends heavily on the pH. So the desorption process of Cr(VI) involves enhancement of the solution pH.

4. Conclusions

In the current study, hybrid Fe–carbon dots were fabricated from molasses precursor using simple microwave method, impregnated with phosphoric acid and activated with $FeCl_3$ followed by pyrolysis under N_2 flow. The morphology of the synthesized carbon dots and hybrid Fe–CDs was investigated using FESEM. EDX analysis was conducted for determining the elemental composition of hybrid Fe–CDs before and after of the Cr(VI) adsorption. The identification of surface functional groups of hybrid nano adsorbent was carried out using FTIR spectra. The specific surface area was calculated to be 2.14 $m^2 g^{-1}$ and 233.7 $m^2 g^{-1}$ for carbon dots and hybrid Fe–CDs respectively, during BET analysis. Using hybrid Fe–CDs as the adsorbent, more than 95% Cr(VI) removal was achieved. The maximum adsorption capacity of Cr(VI) occurred at pH of 2.0 because of the protonation of carbon surface under acidic condition. The adsorption behavior of hybrid Fe–CDs followed both Langmuir (R^2 > 0.996) and Freundlich (R^2 > 0.97) isotherms and Q_m value obtained as 81.97 mg g^{-1}.Adsorption kinetics for Cr(VI) followed the pseudo-second-order model very well and equilibrium was reached after about 90 min. Desorption studies was conducted for five consecutive adsorption-desorption cycles using dilute 1 N NaOH and 1 N HCl aqueous solutions at different initial chromium concentrations of 10 to 100 mg L^{-1}. High desorption efficiency (from 74% to 90.45%) of Cr(VI) was achieved for various initial chromium concentrations. The obtained results confirmed that the synthesized hybrid Fe–CDs is a low-cost and effective adsorbent for the removal of Cr(VI) from contaminated waters. Also, the flexibility and the regeneration of this hybrid nano-adsorbent make it suitable for the application in fixed bed column.

Conflict of interest

The authors have declared no conflict of interest.

Acknowledgement

This article is part of PhD thesis of Azadeh Eslami, PhD candidate of science research branch of Islamic Azad University. The authors appreciate the valuable comments and suggestions from the anonymous reviewers.

References

[1] K. Wang, G. Qiu, H. Cao, R. Jin, Removal of chromium (VI) from aqueous solutions using Fe_3O_4 magnetic polymer micro spheres functionalized with amino groups, Mater., 8 (2015) 8378–8391.

[2] D. Dutta, S. Thiyagarajan, D. Bahadur, SnO_2 quantum dots decorated reduced graphene oxide nano composites for efficient water remediation, Chem. Eng. J., 297 (2016) 55–65.
[3] I.U. Salihi, S.R.M. Kutty, M.H. Isa, Adsorption of lead ions onto activated carbon derived from Sugarcane bagasse. In IOP Conference Ser.: Mater. Sci. Eng., 201(1) (2017) 012034. IOP Publishing.
[4] L.A. Giusto, F.L. Pissetti, T.S. Castro, F. Magalhães, Preparation of activated carbon from Sugarcane bagasse soot and methylene blue adsorption, Water Air Soil Pollut., 228 (2017) 249.
[5] S. Rajput, C.U. Pittman, D. Mohan, Magnetic magnetite (Fe_3O_4) nano particle synthesis and applications for lead (Pb^{2+}) and chromium (Cr^{6+}) removal from water, J. Colloid Interface Sci., 468 (2016) 334–346.
[6] J. Zhou, Y. Wang, J. Wang, W. Qiao, D. Long, L. Ling, Effective removal of hexavalent chromium from aqueous solutions by adsorption on mesoporous carbon micro spheres, J. Colloid Interface Sci., 462 (2016) 200–207.
[7] E. Petala, K. Dimos, A. Douvalis, T. Bakas, J. Tucek, R. Zbořil, M.A. Karakassides, Nanoscale zero-valent iron supported on mesoporous silica: Characterization and reactivity for Cr (VI) removal from aqueous solution, J. Hazard. Mater., 261 (2013) 295–306.
[8] Z. Yan, Z. Zhang, J. Chen, Biomass-based carbon dots: Synthesis and application in imatinib determination, Sens. Actuators, B., 225 (2016) 469–473.
[9] S. Li, L. Liu, Y. Yu, G. Wang, H. Zhang, A. Chen, Fe_3O_4 modified mesoporous carbon nano spheres: Magnetically separable adsorbent for hexavalent chromium, J. Alloys Compd., 698 (2017) 20–26.
[10] B. Qiu, H. Gu, X. Yan, J. Guo, Y. Wang, D. Sun, Q. Wang, M. Khan, X. Zhang, B.L. Weeks, D.P. Young, Cellulose derived magnetic mesoporous carbon nano composites with enhanced hexavalent chromium removal, J. Mater. Chem. A., 2(41) (2014) 17454–17462.
[11] G. Wang, S. Wang, W. Sun, Z. Sun, S. Zheng, Synthesis of a novel illite@ carbon nano composite adsorbent for removal of Cr (VI) from wastewater, J. Environ. Sci., 57 (2017) 62–71.
[12] Y. Du, L. Wang, J. Wang, G. Zheng, J. Wu, H. Dai, Flower, wire, and sheet-like MnO_2-deposited diatomites: Highly efficient absorbents for the removal of Cr (VI), J. Environ. Sci., 29 (2015) 71–81.
[13] X. Sun, L. Yang, Q. Li, J. Zhao, X. Li, X. Wang, H. Liu, Amino-functionalized magnetic cellulose nano composite as adsorbent for removal of Cr (VI): synthesis and adsorption studies, Chem. Eng. J., 241 (2014) 175–183.
[14] Q. Chen, Z. Luo, C. Hills, G. Xue, M. Tyrer, Precipitation of heavy metals from wastewater using simulated flue gas: sequent additions of fly ash, lime and carbon dioxide, Water Res., 43(10) (2009) 2605–2614.
[15] A. Naeem, M.T. Saddique, S. Mustafa, Y. Kim, B. Dilara, Cation exchange removal of Pb from aqueous solution by sorption onto NiO, J. Hazard. Mater., 168(1) (2009) 364–368.
[16] X. Cheng, N. Li, M. Zhu, L. Zhang, Y. Deng, C. Deng, Positively charged microporous ceramic membrane for the removal of Titan Yellow through electrostatic adsorption, J. Environ. Sci., 44 (2016) 204–212.
[17] Y.X. Liu, D.X. Yuan, J.M. Yan, Q.L. Li, T. Ouyang, Electrochemical removal of chromium from aqueous solutions using electrodes of stainless steel nets coated with single wall carbon nanotubes, J. Hazard. Mater., 186(1) (2011) 473–480.
[18] M. Owlad, M.K. Aroua, W.A.W. Daud, S. Baroutian, Removal of hexavalent chromium-contaminated water and wastewater: a review, Water Air Soil Pollut., 200(1–4) (2009) 59–77.
[19] M. Kaur, M. Singh, S.S. Mukhopadhyay, D. Singh, M. Gupta, Structural, magnetic and adsorptive properties of clay ferrite nano composite and its use for effective removal of Cr (VI) from water, J. Alloys Compd., 653 (2015) 202–211.
[20] N. Zaitseva, V. Zaitsev, A. Walcarius, Chromium (VI) removal via reduction–sorption on bi-functional silica adsorbents. J. Hazard. Mater., 250 (2013) 454–461.
[21] J.L. Lv, W. Zheng, Y. Fan, Z.M. Lei, S.R. Zhai, Multi functional hierarchical cabbage-like nZVI-Fe_3O_4/C composites for efficient chromium (VI) removal, J. Taiwan Inst. Chem. Eng., 65 (2016) 312–322.
[22] T. Yang, Y.K. Li, M.L. Chen, J.H. Wang, Supported carbon dots decorated with metallothione in for selective cadmium adsorption and removal, Chin. Chem. Lett., 26(12) (2015) 1496–1501.
[23] X.S. Wang, L. Zhu, H.J. Lu, Surface chemical properties and adsorption of Cu (II) on nano scale magnetite in aqueous solutions, Desalination, 276 (2011) 154–160.
[24] A. Uheida, G. Salazar-Alvarez, E. Björkman, Z. Yu, M. Muhammed, Fe_3O_4 and γ-Fe_2O_3 nano particles for the adsorption of Co^{2+} from aqueous solution, J. Colloid Interface Sci., 298(2) (2006) 501–507.
[25] J. Zhu, H. Gu, J. Guo, M. Chen, H. Wei, Z. Luo, H.A. Colorado, N. Yerra, D. Ding, T.C. Ho, N. Haldolaarachchige, Mesoporous magnetic carbon nano composite fabrics for highly efficient Cr (VI) removal, J. Mater. Chem. A., 2(7) (2014) 2256–2265.
[26] N.N. Nassar, Rapid removal and recovery of Pb(II) from wastewater by magnetic nano adsorbents, J. Hazard. Mater., 184(1) (2010) 538–546.
[27] P.Z.Z. Ngu, S.P.P. Chia, J.F.Y. Fong, S.M. Ng, Synthesis of carbon nano particles from waste rice husk used for the optical sensing of metal ions, New Carbon Mater., 31(2) (2016) 135–143.
[28] B. Das, P. Dadhich, P. Pal, P.K. Srivas, K. Bankoti, S. Dhara, Carbon nano dots from date molasses: new nano lights for the in vitro scavenging of reactive oxygen species, J. Mater. Chem. B., 2(39) (2014) 6839–6847.
[29] S. Sahu, B. Behera, T.K. Maiti, S. Mohapatra, Simple one-step synthesis of highly luminescent carbon dots from orange juice: application as excellent bio-imaging agents, Chem. Commun., 48 (2012) 8835–8837.
[30] M. Zhang, Q. Yao, C. Lu, Z. Li, W. Wang, Layered double hydroxide–carbon dot composite: high-performance adsorbent for removal of anionic organic dye, ACS Appl. Mater. Interfaces., 6(22) (2014) 20225–20233.
[31] R. Liu, J. Liu, W. Kong, H. Huang, X. Han, X. Zhang, Y. Liu, Z. Kang, Adsorption dominant catalytic activity of a carbon dots stabilized gold nano particles system, Dalton Trans., 43(28) (2014) 10920–10929.
[32] J. Wang, W. Zhang, X. Yue, Q. Yang, F. Liu, Y. Wang, D. Zhang, Z. Li, J. Wang, One-pot synthesis of multi functional magnetic ferrite–MOS_2–carbon dot nano hybrid adsorbent for efficient Pb (II) removal, J. Mater. Chem. A., 4(10) (2016) 3893–3900.
[33] L. Wang, C. Cheng, S. Tapas, J. Lei, M. Matsuoka, J. Zhang, F. Zhang, Carbon dots modified mesoporous organo silica as an adsorbent for the removal of 2, 4-dichlorophenol and heavy metal ions, J. Mater. Chem. A., 3(25) (2015) 13357–13364.
[34] D. Dutta, D. Thakur, D. Bahadur, SnO_2 quantum dots decorated silica nano particles for fast removal of cationic dye (methylene blue) from wastewater, Chem. Eng. J., 281 (2015) 482–490.
[35] W. Yao, X. Wang, Y. Liang, S. Yu, P. Gu, Y. Sun, C. Xu, J. Chen, T. Hayat, A. Alsaedi, X. Wang, Synthesis of novel flower-like layered double oxides/carbon dots nano composites for U (VI) and 241Am (III) efficient removal: Batch and EXAFS studies, Chem. Eng. J., 332 (2018) 775–786.
[36] J. Zhang, X. Zhang, S. Dong, X. Zhou, S. Dong, N-doped carbon quantum dots/TiO_2 hybrid composites with enhanced visible light driven photo catalytic activity toward dye wastewater degradation and mechanism insight, J. Photochem. Photobiol. A., 325 (2016) 104–110.
[37] U. Baruah, A. Konwar, D. Chowdhury, A sulphonated carbon dot–chitosan hybrid hydrogel nano composite as an efficient ion-exchange film for Ca^{2+} and Mg^{2+} removal, Nano scale, 8(16) (2016) 8542–8546.
38] Z. Wang, C. Xu, Y. Lu, F. Wu, G. Ye, G. Wei, T. Sun, J. Chen, Visualization of adsorption: luminescent mesoporous silica-carbon dots composite for rapid and selective removal of U (VI) and in situ monitoring the adsorption behavior, ACS Appl. Mater. Interfaces., 9(8) (2017) 7392–7398.
[39] J. Bai, C. Sun, X. Jiang, Carbon dots-decorated multi walled carbon nano tubes nano composites as a high-performance electrochemical sensor for detection of H_2O_2 in living cells, Anal. Bioanal. Chem., 408(17) (2016) 4705–4714.
[40] L.M. Ang, T.A. Hor, G.Q. Xu, C.H. Tung, S.P. Zhao, J.L. Wang, Decoration of activated carbon nanotubes with copper and nickel, Carbon, 38(3) (2000) 363–372.

[41] W. Cui, Q. Liu, N. Cheng, A.M. Asiri, X. Sun, Activated carbon nanotubes: a highly-active metal-free electrocatalyst for hydrogen evolution reaction, Chem. Commun., 50(66) (2014) 9340–9342.
[42] L. Dai, Y. Jiang, W. Meng, H. Zhou, L. Wang, Z. He, Improving the electrocatalytic performance of carbon nanotubes for VO^{2+}/VO^{2+} redox reaction by KOH activation, Appl. Surf. Sci., 401 (2017) 106–113.
[43] C. Bouchelta, M.S. Medjram, O. Bertrand, J.P. Bellat, Preparation and characterization of activated carbon from date stones by physical activation with steam, J. Anal. Appl. Pyrolysis., 82(1) (2008) 70–77.
[44] S.K. Theydan, M.J. Ahmed, Adsorption of methylene blue onto biomass-based activated carbon by $FeCl_3$ activation: equilibrium, kinetics, and thermodynamic studies, J. Anal. Appl. Pyrolysis., 97 (2012) 116–122.
[45] Y. Sun, Q. Yue, Y. Mao, B. Gao, Y. Gao, L. Huang, Enhanced adsorption of chromium onto activated carbon by microwave-assisted H_3PO_4 mixed with Fe/Al/Mn activation, J. Hazard. Mater., 265 (2014) 191–200.
[46] J. Xue, L. Huang, F. Jin, Q. Liu, G. Liu, M. Wang, G. Li, S. Zhou, Two novel and simple strategies for improvement of the traditional activation method for activated carbon preparation: nano-copper catalysis and Cu (II) doping, RSC Adv., 5(100) (2015) 81857–81865.
[47] A.L. Cazetta, O. Pezoti, K.C. Bedin, T.L. Silva, A. Paesano Junior, T. Asefa, V.C. Almeida, Magnetic activated carbon derived from biomass waste by concurrent synthesis: efficient adsorbent for toxic dyes, ACS Sustain. Chem. Eng., 4(3) (2016) 1058–1068.
[48] T. Budinova, E. Ekinci, F. Yardim, A. Grimm, E. Björnbom, V. Minkova, M. Goranova, Characterization and application of activated carbon produced by H_3PO_4 and water vapor activation, Fuel Process. Technol., 87(10) (2006) 899–905.
[49] E. Yagmur, M. Ozmak, Z. Aktas, A novel method for production of activated carbon from waste tea by chemical activation with microwave energy, Fuel, 87(15) (2008) 3278–3285.
[50] I.A.W. Tan, J.C. Chan, B.H. Hameed, L.L.P. Lim, Adsorption behavior of cadmium ions onto phosphoric acid-impregnated microwave-induced mesoporous activated carbon, J. Water Process Eng., 14 (2016) 60–70.
[51] I.A.W. Tan, J.C. Chan, B.H. Hameed, L.L.P. Lim, Adsorption behavior of cadmium ions onto phosphoric acid-impregnated microwave-induced mesoporous activated carbon, J. Water Process Eng., 14 (2016) 60–70.
[52] L. Huang, Y. Sun, T. Yang, L. Li, Adsorption behavior of Ni (II) on lotus stalks derived active carbon by phosphoric acid activation, Desalination, 268(1) (2011) 12–19.
[53] L. Huang, Y. Sun, W. Wang, Q. Yue, T. Yang, Comparative study on characterization of activated carbons prepared by microwave and conventional heating methods and application in removal of oxytetracycline (OTC), Chem. Eng. J., 171(3) (2011) 1446–1453.
[54] M. Bhaumik, A. Maity, V.V. Srinivasu, M.S. Onyango, Removal of hexavalent chromium from aqueous solution using polypyrrole-polyaniline nanofibers, Chem. Eng. J., 181 (2012) 323–333.
[55] H.P. Boehm, Surface oxides on carbon and their analysis: a critical assessment, Carbon, 40(2) (2002) 145–149.
[56] G.Z. Zhu, X.L. Deng, M. Hou, K. Sun, Y.P. Zhang, P. Li, F.M. Liang, Comparative study on characterization and adsorption properties of activated carbons by phosphoric acid activation from corncob and its acid and alkaline hydrolysis residues, Fuel Process. Technol., 144 (2016) 255–261.
[57] Z.A. ALOthman, A review: fundamental aspects of silicate mesoporous materials, Mater., 5(12) (2012) 2874–2902.
[58] M. Avila, T. Burks, F. Akhtar, M. Göthelid, P.C. Lansåker, M.S. Toprak, M. Muhammed, A. Uheida, Surface functionalized nanofibers for the removal of chromium (VI) from aqueous solutions, Chem. Eng. J., 245 (2014) 201–209.
[59] P.K. Pandey, S.K. Sharma, S.S. Sambi, Kinetics and equilibrium study of chromium adsorption on zeolite NaX, Int. J. Environ. Sci. Technol., 7(2) (2010) 395–404.
[60] I. Langmuir, The constitution and fundamental properties of solids and liquids. II. Liquids, J. Am. Chem. Soc., 39(9) (1917) 1848–1906.
[61] H.M.F. Freundlich, Over the adsorption in solution, J. Phys. Chem., 57 (1906) 1100–1107.
[62] S.A. Pathan, N.S. Pandita, Nanoporous carbon synthesized from grass for removal and recovery of hexavalent chromium, Carbon. Lett., 20(1) (2016) 10–18.
[63] M.S. Miao, Q. Liu, L. Shu, Z. Wang, Y.Z. Liu, Q. Kong, Removal of cephalexin from effluent by activated carbon prepared from alligator weed: Kinetics, isotherms, and thermodynamic analyses, Process Saf. Environ. Prot., 104 (2016) 481–489.
[64] S. Dubey, D. Gusain, Y.C. Sharma, Kinetic and isotherm parameter determination for the removal of chromium from aqueous solutions by nanoalumina, a nanoadsorbent, J. Mol. Liq., 219 (2016) 1–8.
[65] S. Yang, L. Li, Z. Pei, C. Li, J. Lv, J. Xie, B. Wen, S. Zhang, Adsorption kinetics, isotherms and thermodynamics of Cr (III) on graphene oxide, Colloids Surf., A, 457 (2014) 100–106.
[66] H. Mittal, N. Ballav, S.B. Mishra, Gum ghatti and Fe_3O_4 magnetic nanoparticles based nanocomposites for the effective adsorption of methylene blue from aqueous solution, J. Ind. Eng. Chem., 20(4) (2014) 2184–2192.
[67] J.N. Tiwari, K. Mahesh, N.H. Le, K.C. Kemp, R. Timilsina, R.N. Tiwari, K.S. Kim, Reduced graphene oxide-based hydrogels for the efficient capture of dye pollutants from aqueous solutions, Carbon, 56 (2013) 173–182.
[68] Y. Yao, S. Miao, S. Liu, L.P. Ma, H. Sun, S. Wang, Synthesis, characterization, and adsorption properties of magnetic Fe_3O_4@graphene nanocomposite, Chem. Eng. J., 184 (2012) 326–332.
[69] J. Zhang, T. Shang, X. Jin, J. Gao, Q. Zhao, Study of chromium (VI) removal from aqueous solution using nitrogen-enriched activated carbon based bamboo processing residues, RSC Adv., 5(1) (2015) 784–790.
[70] M.K. Rai, G. Shahi, V. Meena, R. Meena, S. Chakraborty, R.S. Singh, B.N. Rai, Removal of hexavalent chromium Cr (VI) using activated carbon prepared from mango kernel activated with H_3PO_4, Resour.-Effic. Technol., 2 (2016) S63–S70.